Experimental measurement of the scale-by-scale momentum transport budget in a turbulent shear flow

L. Marié and F. Daviaud[a)]
GIT/SPEC, DSM, CEA/Saclay, 91191 Gif-sur-Yvette Cedex, France

(Received 21 April 2003; accepted 20 October 2003; published online 8 January 2004)

We report measurements linking velocity fluctuations with the turbulent drag in a turbulent closed flow, namely the von Kármán flow. Making use of the angular momentum balance equation in integral form, we obtain a simple expression for the torque applied by the forcing mechanism, which we check against quantitative laser Doppler velocimetry measurements. We then decompose the angular momentum flux into contributions coming from the different spectral components of the flow. We provide evidence of the fact that the turbulent drag is dominantly generated by coherent structures at the largest scales of the flow. © *2004 American Institute of Physics.*
[DOI: 10.1063/1.1637602]

I. INTRODUCTION

Since the seminal work of Kolmogorov, considerable work has been devoted to the study of statistical quantities describing isotropic and homogeneous small-scale turbulence (see, e.g., Refs. 1 and 2 for a review). Evidence of universality has been found in many cases, while small-scale intermittency has been found in various quantities such as passive scalar dynamics, velocity increments, or dissipation of energy.[3–5] In the meantime, coherent structures and large scales have also received attention, from a theoretical and an experimental standpoint, while the use of large eddy simulation has become widespread in the field of engineering. Both small[6] and large scales have been studied in the von Kármán flow, namely the flow generated between two coaxial rotating impellers (for a review, see Ref. 7), which is generally considered as a representative situation in which to study well-developed turbulence. A particular interest has been focused on the study of the power injection,[8,13] whose fluctuations have been found to bear close resemblance to those of energy dissipation fluctuations in other out-of-equilibrium systems.[9] Lately, they have been linked[10] to the dynamics of the discrete vorticity filaments previously discovered experimentally in the same configuration,[11] and numerically in a close situation.[12] However, experimental studies[13] have shown the time-averaged mechanical power consumption to be quite different from the volume integral of the turbulent dissipation, estimated from pressure fluctuations. In this article, using a new approach based on angular momentum conservation arguments, we present experimental results linking the time-averaged value of the drag torque to velocity fluctuation correlations in the von Kármán flow. Measuring the cospectrum of the velocity fluctuations, we present evidence that the drag torque is dominantly associated with the large-scale dynamics of the flow.

II. THE EXPERIMENTAL SETUP

Our experimental setup is represented in Fig. 1(a). It consists of a Plexiglas™ cylinder, 200 mm in diameter and 300 mm in height, filled with water. Two impellers, each consisting of a flat disc fitted with blades, are located 180 mm apart, at both ends (cf. Table I). The impellers are driven, with the help of belts, by two 1.8 kW brushless motors, which allow rotation rates of up to 20 Hz to be achieved, depending on the configuration. If we take the distance between the discs as a length scale, and the rim velocity achieved at $\Omega_1=\Omega_2=1$ Hz with the smallest impellers as a typical velocity, we can see that $\mathrm{Re}\simeq 8.5\times 10^4$. We can thus assume that, for all the results presented here, the flow is in a state of fully developed turbulence. The variable frequency drives used to control the motors also allow us to measure directly the angular velocities (respectively, mechanical torques) with an accuracy better than 0.5% (respectively, 5%). We have performed calibration runs without impellers, in order to correct the torque measurements for the torque induced by friction in the sealings and bearings. Velocity measurements were performed using a one-component Dantec LDV system.

III. ANGULAR MOMENTUM BALANCE

In the following we adapt the classical derivation[14] of the drag induced by the wake of an object to our particular flow configuration. The rate of change of the z component of the angular momentum of the matter (including the impeller) contained in the volume $\mathbf{V}(z)$ of Fig. 1(a) is given by (see, e.g., Ref. 15)

$$\frac{d}{dt}\int_{\mathbf{V}(z)}\rho r v_\theta d^3\tau = -\int_{\Sigma(z)}\rho r v_\theta v_z d^2S + \int_{\Sigma(z)} r\sigma_\theta d^2S + \int_{\Sigma_b} r\sigma_\theta d^2S + \int_{\mathbf{S}(z)} r\sigma_\theta d^2S + \int_{\mathbf{V}(z)} r f_\theta d^3\tau, \quad (1)$$

where ρ is the volumic mass at the integration point, f_θ is the θ component of the volume forces at the integration point, and σ_θ is the θ component of the surface forces exerted by the environment on the fluid at the integration point on the surfaces. In our laboratory experiment, we can assume rf_θ to

a)Electronic mail: daviaud@drecam.saclay.cea.fr

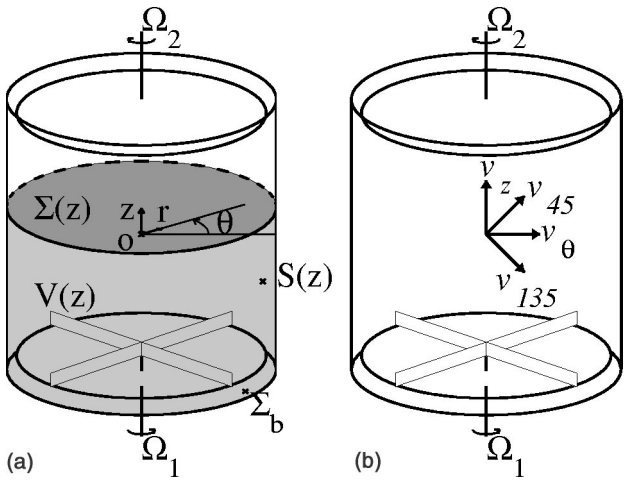

FIG. 1. Experimental setup: (a) $\mathbf{V}(z)$ denotes the control volume used for the momentum balance equation. It is bounded on the sides by $\mathbf{S}(z)$, at the top by $\Sigma(z)$, and at the bottom by Σ_b. (b) Directions of laser Doppler velocimetry measurements (see the text for details).

integrate to zero. Part of the stresses on Σ_b stems from the elastic stress distribution in the impeller shaft, at the point where the shaft enters $\mathbf{V}(z)$. This part we will denote by Γ_1. The angular momentum balance equation applied to the volume of the shaft outside $\mathbf{V}(z)$, the belt and the pulleys then shows that the time average of Γ_1 is equal to the time-averaged mechanical torque supplied by motor 1, minus the friction torque in the bearings and the sealing. On the remaining part of Σ_b, on $\mathbf{S}(z)$ and on $\Sigma(z)$, the stresses come either from viscosity, or from the θ component of pressure gradients. Integrating the θ derivative of the pressure on either of these surfaces yields zero. The time average of the viscous stresses exerted by the vessel on the fluid through $\mathbf{S}(z)$ and Σ_b we will denote by $\Gamma_v(z)$. Performing the usual Reynolds decomposition of the instantaneous velocity $\vec{v}(t)$ into a time-averaged part $\vec{V}$ and a fluctuating part $\vec{v}$ such that $\langle \tilde{v} \rangle = 0$,[2] and eventually taking the time average of Eq. (1), one obtains

$$\int_{\Sigma(z)} \rho \langle r \tilde{v}_\theta \tilde{v}_z \rangle d^2S + \int_{\Sigma(z)} \rho r V_\theta V_z d^2S = \mu \int_{\Sigma(z)} r \partial_z V_\theta d^2S + \Gamma_1 + \Gamma_v(z), \tag{2}$$

where $\langle q \rangle$ denotes the time average of quantity q and μ is the dynamic viscosity of the fluid. It is easy to see that the ratio of the inertial terms of the left-hand side of Eq. (2) to the first term of the right-hand side is of the order of magnitude of the Reynolds number of the flow. In the very turbulent regime achieved in our experiment, this term is then negligible compared to the other terms. Such arguments do not apply to the viscous term $\Gamma_v(z)$, but we have observed *a posteriori* that its contribution remains small in the overall balance, at least in the case of perfect counter-rotation, if the discs have blades. We finally get

$$\Gamma_1 = -\Gamma_v(z) + \int_{\Sigma(z)} \rho \langle r \tilde{v}_\theta \tilde{v}_z \rangle d^2S + \int_{\Sigma(z)} \rho r V_\theta V_z d^2S. \tag{3}$$

Equation (3) shows that the angular momentum transmitted by the motor to the fluid comprised in $\mathbf{V}(z)$ is either evacuated to the walls through $\Gamma_v(z)$ or transported to the fluid contained in the remaining part of the vessel, where it will either be evacuated to the walls, or received by motor 2 as drag.

TABLE I. Characteristics of the different impellers. D is the diameter of the disc, h is the height of the blades, r_c is the blade curvature radius.

Impeller	D (mm)	# blades	h (mm)	r_c (mm)
TM60a	185	16	10	49
TM60b	185	16	20	49
TM70	146	8	20	Straight

IV. MEASUREMENTS

In order to measure the different terms of Eq. (3), we have performed LDV measurements in the plane $\Theta = 0$ of Fig. 1(a). The grid had a 10 mm mesh in the axial and radial directions, and did not cover the part of the volume that was swept by the impeller blades. We have performed the measurements for five different configurations, at the quite low angular speed of 2 Hz, so as to avoid excessive heating of the water. In order to measure the correlation $\langle \tilde{v}_\theta \tilde{v}_z \rangle$ with our one-component LDV setup, we have performed successive measurements in the different directions shown in Fig. 1(b). Apart from coefficients arising from the refraction effects, which were taken care of in the data processing, $v_{45} \simeq (v_\theta + v_z)/\sqrt{2}$, and $v_{135} \simeq (v_\theta - v_z)/\sqrt{2}$. The variances of v_{45} and v_{135} are then given by: $2\langle \tilde{v}_{45}^2 \rangle = \langle \tilde{v}_\theta^2 \rangle + \langle \tilde{v}_z^2 \rangle + 2\langle \tilde{v}_\theta \tilde{v}_z \rangle$ and $2\langle \tilde{v}_{135}^2 \rangle = \langle \tilde{v}_\theta^2 \rangle + \langle \tilde{v}_z^2 \rangle - 2\langle \tilde{v}_\theta \tilde{v}_z \rangle$. Combining the experimentally measured variances thus allowed us to obtain several redundant estimations of the correlation $\langle \tilde{v}_\theta \tilde{v}_z \rangle$ at each point. Assuming time-averaged flow quantities to be axisymmetric [which is not true of instantaneous quantities, as is obvious from the photograph in Fig. 3(d)], we were then able to evaluate numerically the integrals of Eq. (3). Table II displays the z-averaged values of the total angular momentum flux, estimated in three different ways, together with the values obtained through direct torque measurement, in the different flow configurations. The agreement between the direct mechanical torque measurements and the velocity measurements is very good. This proves that the viscous term $\Gamma_v(z)$, which we have not been able to take into account, is small enough to be neglected. This also suggests that our approach could provide a way to evaluate flow-induced forces in cases where direct measurement is difficult. Figure 2 shows, at each axial position z, the two inertial terms of Eq. (3) for the impeller named TM60a, rotating in the forward direction. An important feature of the curves of Fig. 2 is that, half-way between the discs, the part of the angular momentum carried by the mean flow vanishes. At this point, the sole turbulent fluctuations are responsible for the whole of the angular momentum flux. In Fig. 3, we show the results of the LDV measurements for the same impellers. Figure 3(a) represents the distribution of time-averaged flow velocities in the mea-

TABLE II. Angular momentum flux measurements for the different impellers. Φ_1, Φ_2, Φ_3 have been obtained using $\langle \tilde{v}_\theta \tilde{v}_z \rangle = \langle \tilde{v}_\theta^2 \rangle/2 + \langle \tilde{v}_z^2 \rangle/2 - \langle \tilde{v}_{135}^2 \rangle$, $\langle \tilde{v}_\theta \tilde{v}_z \rangle = \langle \tilde{v}_{45}^2 \rangle - \langle \tilde{v}_\theta^2 \rangle/2 - \langle \tilde{v}_z^2 \rangle/2$, $\langle \tilde{v}_\theta \tilde{v}_z \rangle = (\langle \tilde{v}_{45}^2 \rangle - \langle \tilde{v}_{135}^2 \rangle)/4$. Γ_1 (respectively, Γ_2) is the torque applied by motor 1 (respectively, motor 2), obtained by direct measurement.

Velocity field	TM70	TM60a	TM60a (reverse)	TM60b	TM60b (reverse)
Φ_1 (10^{-2} N m)	9.32 ± 0.58	3.60 ± 0.13	-11.70 ± 0.87	9.55 ± 0.55	-23.1 ± 1.8
Φ_2 (10^{-2} N m)	10.52 ± 0.52	4.94 ± 0.20	-11.76 ± 0.26	9.58 ± 0.72	-21.5 ± 0.4
Φ_3 (10^{-2} N m)	9.92 ± 0.49	4.27 ± 0.13	-11.73 ± 0.46	9.56 ± 0.62	-22.3 ± 1.0
$(\Gamma_1+\Gamma_2)/2$ (10^{-2} N m)	9.5 ± 1	3.9 ± 1	-13.3 ± 1	8.7 ± 1	-22.2 ± 1

surement plane. We can see that the meridian circulation has the shape of two distinct cells. The axial velocities are directed toward the impellers close to the cylinder axis, and away from the impellers close to the cylinder wall. In each cell, the azimuthal velocity is imposed by the rotation of the closest impeller. To recover the radial component of the velocity, which is difficult to measure for practical reasons, we have used the incompressibility relationship, assuming again all time-averaged quantities to be axisymmetric. The accuracy of this post-processing step is difficult to evaluate, but is not critical for our purposes, since Eq. (3) does not involve the radial velocity. We can see in Fig. 3(a) that both V_θ and V_z vanish in the midplane of the flow. Figure 3(b) shows that their product consequently also vanishes. Another interesting feature of Fig. 3(b) is that we can see that the positive values of $rV_\theta V_z$ are concentrated in a thin cylindrical volume, close to the vessel wall, while weakly negative values occupy the core of the flow. These negative values add up to form a backwards flow of angular momentum, directed from impeller 2 (top) to impeller 1 (bottom). The magnitude of this flow is roughly half that of the mechanical torque supplied by impeller 1. In Fig. 3(c), we show the spatial distribution of the velocity correlation, multiplied by the radial position r. We observe that the correlation is important mainly in a region located half-way between the two discs, close to the cylinder wall. We have performed flow visualizations, using air bubbles as tracer particles. In the region of the flow where large correlations are present, we have observed large coherent structures, very similar in shape to the ones reported in Ref. 16 in a turbulent mixing layer. These structures, which have already been mentioned in Ref. 17, have the shape of a succession of large (5–10 cm) corotating radial vortices, superimposed on a background of developed turbulent motion. We believe that they are produced by an instability of the global circulation of the flow, whose mechanism is probably akin to that of the Kelvin–Helmoltz mixing layer instability. The photograph in Fig. 3(d) shows a typical coherent vortex, in the flow generated by the same impellers, at the higher rotation speed of $\Omega_1 = \Omega_2 = 15$ Hz, i.e., for $\mathrm{Re} \simeq 1.6 \times 10^6$. These vortices move slowly as a whole in one direction or the other, and seem to appear or merge randomly, with a lifetime of the order of a few seconds. They seem to exist even for $\mathrm{Re} < 1000$ in a setup that uses silicon oil ($\nu = 10^{-4}$ m^2 s^{-1}), as well as in the simulations of Ref. 18.

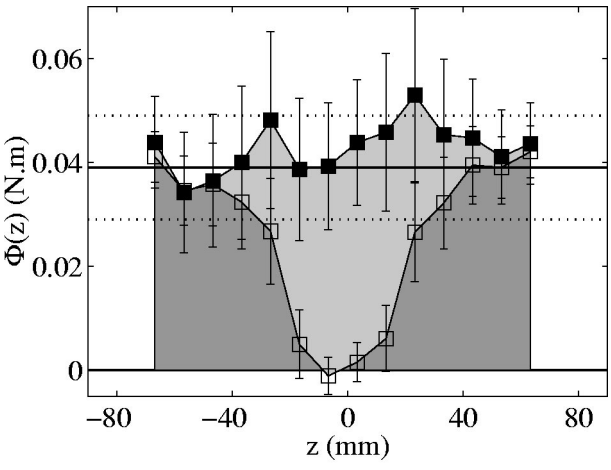

FIG. 2. Contributions of the different inertial terms of Eq. (3) to the angular momentum flux $\Phi(z)$ across $\Sigma(z)$. The open (respectively, closed) squares correspond to the angular momentum transported by the mean flow (respectively, mean flow plus fluctuations). The darker (respectively, lighter) area represents the part transported by the mean flow (respectively, fluctuations). The lines represent the 5% accuracy bounds on the direct torque measurement. The large uncertainty is due to the static torque in bearings and sealings (~0.2 N m).

V. SCALE-BY-SCALE BUDGET OF MOMENTUM TRANSPORT

A further step is then to decompose the velocity correlation $\langle \tilde{v}_\theta \tilde{v}_z \rangle$ into the contributions coming from the different spectral components contained in $v_\theta(t)$ and $v_z(t)$. Denoting the temporal Fourier transform of the quantity q by $\hat{q}(\omega)$, we can write

$$\langle \tilde{v}_0 \tilde{v}_z \rangle + V_\theta V_z = \widehat{v_\theta v_z}(\omega = 0) = \int_{-\infty}^{\infty} \widehat{v_\theta}(\omega) \widehat{v_z}(-\omega) d\omega$$

and then

$$\langle \tilde{v}_\theta \tilde{v}_z \rangle + 2 V_\theta V_z = \int_0^{\infty} 2\Re[\widehat{v_\theta}(\omega) \widehat{v_z}^*(\omega)] d\omega. \quad (4)$$

Measuring the real part of the temporal co-spectrum of the two velocity components v_θ and v_z seems then a natural way to assess the relative importance of eddies of the various (time) scales for the turbulent momentum transport across $\Sigma(z)$.[19] Combining the different velocity components as above, one can obtain the integrand of Eq. (4) as $2\Re(\widehat{v_\theta v_z}^*) = |\widehat{v_{45}}|^2(\omega) - |\widehat{v_{135}}|^2(\omega)$. We have performed careful LDV measurements at the point in the flow where the velocity correlation is largest. In each measurement direction, we have recorded 20 min of velocity signal. Running the experiment at the higher motor frequency of 15 Hz has

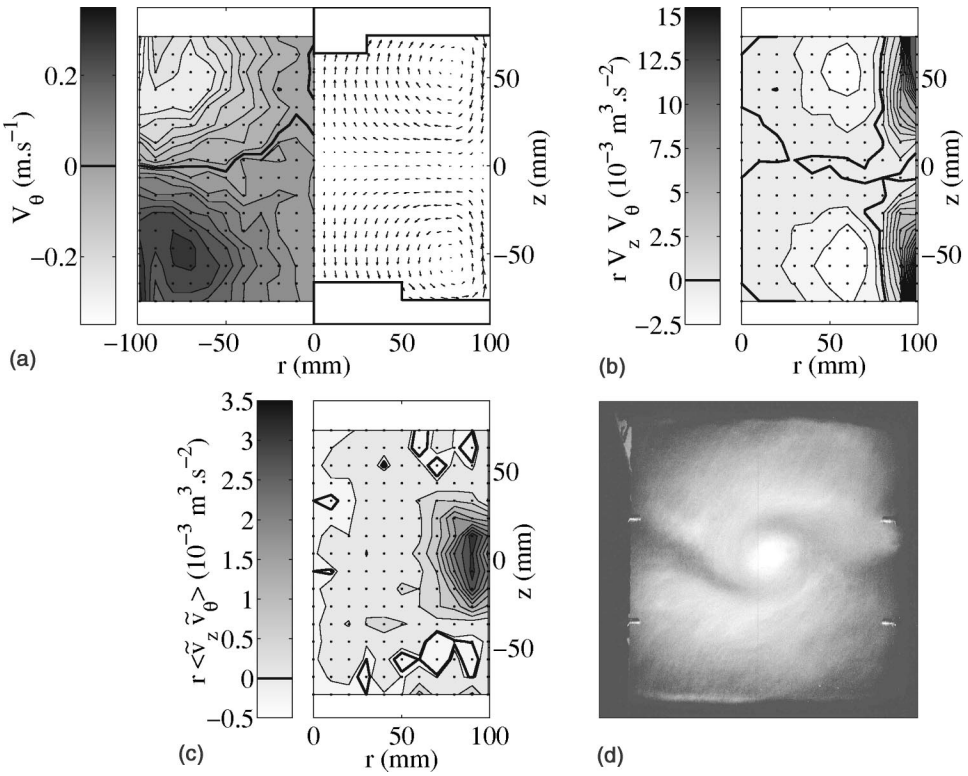

FIG. 3. (a) Spatial distribution of time-averaged velocities. The azimuthal component of the flow is on the left-hand side, while the meridian component is on the right-hand side. The thick black line on the left-hand graph denotes null values of the azimuthal velocities. The white areas in the graphs mark the parts of the flow where the impeller blades precluded measurement. The longest arrow in the right-hand graph is 0.50 m s^{-1} long. The impeller located at the bottom (respectively, top) rotates to the right (respectively, left). Both are of the TM60a type, and rotate at 2 Hz (Re$\simeq 2.1\times 10^5$). (b) Spatial distribution of the product of mean velocities $rV_\theta V_z$. (c) Spatial distribution of the velocity correlation $r\langle \tilde{v}_\theta \tilde{v}_z \rangle$. (d) $\frac{1}{25}$ s exposure time photograph of a coherent vortex near the midplane of the flow. Same viewpoint as for Fig. 1. The impeller located at the bottom (respectively, top) rotates to the right (respectively, left). Both rotate at 15 Hz (Re$\simeq 1.6\times 10^6$). The real-size height is $\sim$180 mm.

allowed a sustained acquisition rate of nearly 1 kHz. The acquired data have then been resampled to 1 kHz using a simple sample-and-hold algorithm.[20]

We have plotted in Fig. 4 the power spectral densities of v_{45} and v_{135}, together with $2\Re(\widehat{v_\theta v_z^*})$. The two power spectral densities are strongly different in magnitude, thus revealing a very strong anisotropy, at least at large time scales. In the low frequency range ($f<1$ Hz), both seem to have a broad peak, roughly located at $f=0.4$ Hz. This could be related to the slow motion of the coherent vortices. In the 1–10 Hz range, the power spectral density of v_{135} decays algebraically, more slowly than that of v_{45}. At $f=10$ Hz, both power spectral densities have a crossover to a steeper algebraic decay. In the whole region up to $f\simeq 30$ Hz, $2\Re(\widehat{v_\theta v_z^*})$ remains positive, indicating a clear excess of events directed along v_{45}.[22] The curve of $2\Re(\widehat{v_\theta v_z^*})$ follows quite closely that of the PSD of v_{45} up to 1 Hz, then starts a faster decay. At the 10 Hz crossover the decay becomes algebraic, but after 30 Hz, the sign is no longer constant, and the log–log plot is no longer accurate. Nevertheless, this decay seems in good agreement with the $-7/3$ decay predicted (in the spatial frequency domain) by Ref. 23. If one plots the integral of Eq. (4) as a function of the higher cut-off frequency f_c, one can see that the result is within 10% of the final correlation value as soon as $f_c>4$ Hz, and that flow fluctuations at frequencies higher than 30 Hz contribute less than 0.5% of the total angular momentum transport at this point. From this we conclude that the angular momentum transport, and thus the drag torque, is mainly produced by the slow flow fluctuations, with time scales larger than roughly 0.1 s.

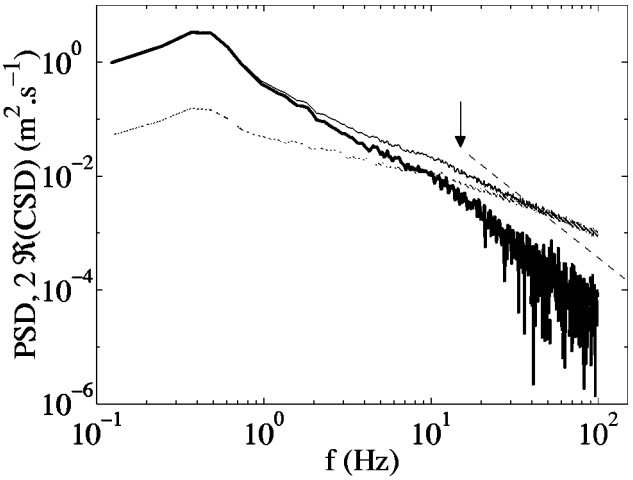

FIG. 4. Power spectral density plots of v_{45} (thin black line) and v_{135} (thin gray line) at $z=0$ mm, $r=90$ mm. The thick black line represents $2\Re(\widehat{v_\theta v_z}^*)$. The data have been obtained with the TM60a impellers, rotating at 15 Hz (Re$\simeq 1.6\times 10^6$). The dotted line we have plotted to guide the eye corresponds to the $-7/3$ slope predicted by Ref. 23, and the arrow corresponds to the impeller angular frequency. Negative values of $2\Re(\widehat{v_\theta v_z}^*)$, which occur after $f>30$ Hz, have not been represented.

VI. CONCLUSION AND REMARKS

We have shown that, even in a fully turbulent flow, use of integral momentum balance equations allows one to find explicit links between flow characteristics and momentum injection by the forcing mechanism.[2,14] This kind of approach can provide tools for the evaluation of flow-induced forces in cases where direct measurement is difficult. We have also provided quantitative evidence of the fact that a major part of the turbulent shear stresses are generated by flow fluctuations at the largest scales of the flow. We believe this result is not specific to the von Kármán geometry, but also applies in other free shear flows presenting large-scale structures, such as the plane mixing layer, the turbulent jet, or the Kármán vortex street. The coherent structures present in these flows can be expected to have a strong influence, this time on linear momentum transport. These structures should also be amenable to simulation, as suggested by Ref. 24, based on numerical evidence.

We will now present critical remarks to show possible directions that may deserve further study. Our first remark concerns the turbulent normal stresses. Using the z component of the integral momentum equation, one can derive the force exerted by the fluid in $\mathbf{V}(z)$ on the rest of the fluid as the surface integral of ρv_z^2 on $\Sigma(z)$. It is theoretically well known[1] that small-scale motions can still contribute in a non-negligible way to this integral. This draws a clear distinction between less documented, large-scale dominated, turbulent shear stresses and turbulent normal stresses, which are generated at all scales, but for which a considerable amount of theoretical knowledge is already available. Second, we wish to stress the need for a proper understanding of the injection of momentum to the flow through viscous boundary layers. Indeed, in the process of applying the angular momentum balance equation, we have not been able to consider properly the viscous torque exerted on the fluid by the cylinder wall. Though, in the case of perfect counter-rotation, we have found its influence to be small, we have observed that in other situations it can be responsible for a large share ($\sim$20%) of the drag torque. We can also expect that in cells with larger aspect ratio (i.e., larger distance between the impellers) it could induce ''angular momentum leaks,'' which would slightly affect the quality of the match between LDV measurements and mechanical torque measurements. Finally, we think that, since the large scales are responsible for a dominant part of the momentum transfer, their dynamics can be expected to bear a strong influence on the energy injection fluctuations studied by in Refs. 8–10.

ACKNOWLEDGMENTS

The authors thank B. Castaing, A. Chiffaudel, O. Dauchot, B. Dubrulle, S. Fauve, J.-F. Pinton, and C. Titon for fruitful discussion, and C. Gasquet and V. Padilla for technical assistance.

[1] U. Frisch, *Turbulence* (Cambridge University Press, Cambridge, 1995).
[2] J. O. Hinze, *Turbulence* (McGraw–Hill, New York, 1959).
[3] Y. Gagne and B. Castaing, ''Une représentation universelle sans invariance globale d'échelle des spectres d'énergie en turbulence développée,'' C. R. Acad. Sci. (Paris) II **312**, 441 (1991).
[4] F. Anselmet, Y. Gagne, E. Hopfinger, and R. A. Antonia, ''High-order velocity structure functions in turbulence shear flows,'' J. Fluid Mech. **140**, 63 (1984).
[5] F. Moisy, H. Willaime, J. S. Andersen, and P. Tabeling, ''Passive scalar intermittency in low temperature helium flows,'' Phys. Rev. Lett. **86**, 4827 (2001).
[6] P. Tabeling, G. Zocchi, F. Belin, J. Maurer, and H. Willaime, ''Probability density functions, skewness, and flatness in large Reynolds number turbulence,'' Phys. Rev. E **53**, 1613 (1996).
[7] P. J. Zandbergen and D. Dijkstra, ''Von Kármán swirling flows,'' Annu. Rev. Fluid Mech. **19**, 465 (1987).
[8] R. Labbé, J.-F. Pinton, and S. Fauve, ''Power fluctuations in turbulent swirling flows,'' J. Phys. II **6**, 1099 (1996).
[9] S. T. Bramwell, P. C. W. Holdsworth, and J.-F. Pinton, ''Universality of rare fluctuations in turbulence and critical phenomena,'' Nature (London) **396**, 552 (1998).
[10] O. Cadot and C. Titon, ''The statistics of power injected in a closed turbulent flow: Constant torque forcing vs. constant velocity forcing,'' Phys. Fluids **15**, 625 (2003).
[11] S. Douady, Y. Couder, and M.-E. Brachet, ''Direct observation of the intermittency of intense vorticity filaments in turbulence,'' Phys. Rev. Lett. **67**, 983 (1991).
[12] M.-E. Brachet, D. I. Meiron, S. Orszag, B. G. Nickel, R. H. Morf, and U. Frisch, ''Small-scale structure of the Taylor–Green vortex,'' J. Fluid Mech. **130**, 411 (1983).
[13] O. Cadot, Y. Couder, A. Daerr, S. Douady, and A. Tsinober, ''Energy injection in closed turbulent flows: Stirring through boundary layers versus inertial stirring,'' Phys. Rev. E **56**, 427 (1997).
[14] G. K. Batchelor, *An Introduction to Fluid Dynamics* (Cambridge University Press, Cambridge, 1970).
[15] D. J. Acheson, *Elementary Fluid Dynamics* (Clarendon, Oxford, 1990).
[16] G. L. Brown and A. Roshko, ''On density effects and large structures in turbulent mixing layer,'' J. Fluid Mech. **64**, 775 (1974).
[17] G. Zocchi, P. Tabeling, J. Maurer, and H. Willaime, ''Measurement of the scaling of the dissipation at high Reynolds numbers,'' Phys. Rev. E **50**, 3693 (1994).
[18] C. Nore, L. S. Tuckerman, O. Daube, and S. Xin, ''The 1:2 mode interaction in exactly counter-rotating von Kármán swirling flow,'' J. Fluid Mech. **477**, 51 (2003).
[19] J. C. Kaimal, J. C. Wyngaard, Y. Izumi, and O. R. Coté, ''Spectral characteristics of surface-layer turbulence,'' Q. J. R. Meteorol. Soc. **98**, 563 (1972).
[20] Computing the power spectral density of a white-in-time Gaussian noise resampled using the original LDV burst arrival time allows us to assess the cut-off properties of the acquisition process. We have observed that the resampling process does act as a low-pass filter (Ref. 21), but that the power spectral density is affected by less than 0.5 dB for frequencies up to 100 Hz.
[21] P. Buchhave, W. K. George, Jr., and J. L. Lumley, ''The measurement of turbulence with the laser-doppler anemometer,'' Annu. Rev. Fluid Mech. **11**, 443 (1979).
[22] W. W. Willmarth and S. S. Lu, ''Structure of the Reynolds stress near the wall,'' J. Fluid Mech. **55**, 65 (1972).
[23] J. L. Lumley, ''Similarity and the turbulent energy spectrum,'' Phys. Fluids **10**, 855 (1967).
[24] J. Jimenez and R. D. Moser, ''LES: Where are we and what can we expect?'' Aust. J. Phys. Astrophys. Suppl. **38**, 605 (2000).